Internet of Things 34 (2025) 101813

Contents lists available at ScienceDirect

Internet of Things

journal homepage: www.elsevier.com/locate/iot

Reconfigurable intelligent surfaces for enhanced localisation: Advancing performance with KAN-based deep learning models

Abdelghani Dahou [a,b], Syed Tariq Shah [c,*], Insaf Ullah [c], Tahira Mahboob [d], Ahmed Gamal Abdellatif [e], Mohamed Abd Elaziz [f,g], Ahmad Almogren [h,*], Mahmoud A. Shawky [d,i,*]

[a] School of Computer Science and Technology, Zhejiang Normal University, Jinhua, 321004, China
[b] Faculty of Material Sciences, Mathematics and Computer Science, University of Ahmed Draia, Adrar, 01000, Algeria
[c] School of Computer Science and Electronic Engineering, University of Essex, CO4 3SQ, Colchester, UK
[d] School of Computing Science and James Watt School of Engineering, University of Glasgow, G12 8QQ, Glasgow, UK
[e] Faculty of Computers and Information Systems, Egyptian Chinese University, 11765, Cairo, Egypt
[f] Department of Mathematics, Faculty of Science, Zagazig University, Zagazig, 44519, Egypt
[g] Artificial Intelligence Research Center (AIRC), College of Engineering and Information Technology, Ajman University, 11633, Ajman, UAE
[h] Department of Computer Science, College of Computer and Information Science, King Saud University, 11633, Riyadh, Saudi Arabia
[i] The Egyptian Technical Research and Development Centre, 11618, Cairo, Egypt

ARTICLE INFO

Keywords:
Deep learning
Kolmogorov-Arnold networks (KAN)
Localisation
Reconfigurable intelligent surfaces (RIS)
Wireless signal classification

ABSTRACT

Accurate localisation is a critical component in modern wireless communication systems, especially in complex environments with a very low signal-to-noise ratio (SNR). Reconfigurable intelligent surfaces (RIS) have emerged as a promising solution to enhance localisation accuracy by dynamically controlling signal reflection patterns. Motivated by the need for precise localisation solutions, this study introduces the RIS-enhanced hybrid localisation network (RHL-Net), a novel framework that integrates RIS with advanced deep learning techniques. RHL-Net employs long short-term memory (LSTM) networks for temporal data processing and Kolmogorov-Arnold networks (KAN) for spatial feature extraction. The key innovation of using KAN lies in its superior ability to learn complex spatial structures compared to traditional Multi-Layer Perceptrons (MLPs); KANs achieve higher accuracy with significantly fewer parameters and offer greater interpretability through their spline-based activation functions, which are learnable and adaptable. This makes KAN uniquely suited for distilling the intricate spatial fingerprints from the RIS-enhanced channel for precise location estimation. For performance evaluation, RHL-Net uses a dataset acquired from a dual-channel universal software radio peripheral (USRP) system, which records received signal strength (RSS) and channel phase response within a single-input multiple-output (SIMO) orthogonal frequency division multiplexing (OFDM) system. A dual-channel USRP with two antennas at the receiver (Rx) side is deployed at a grid of positions with an interspacing distance (x) to assess the RHL-Net localisation performance. Experimental results show that for $x = 0.5$ metres with Directive and Monopole Rx antenna configurations, RHL-Net achieves average accuracies of 69.00 % and 74.19 %, respectively, with RIS activated, significantly outperforming the deactivated configuration. Similarly, for $x = 1$ metre, Directive and Monopole setups achieve average accuracies of 85.58 % and 73.88 %, respectively, with RIS activation. These results

* Corresponding authors.
E-mail addresses: dahou.abdghani@univ-adrar.edu.dz (A. Dahou), syed.shah@essex.ac.uk (S.T. Shah), insaf.ullah@essex.ac.uk (I. Ullah), Tahira.Mahboob@glasgow.ac.uk (T. Mahboob), Ahmed.Gamal@ecu.edu.eg (A.G. Abdellatif), abd_el_aziz_m@yahoo.com (M. Abd Elaziz), ahalmogren@ksu.edu.sa (A. Almogren), mahmoud.shawky@glasgow.ac.uk (M.A. Shawky).

https://doi.org/10.1016/j.iot.2025.101813
Received 31 May 2025; Received in revised form 4 October 2025; Accepted 23 October 2025
Available online 28 October 2025

demonstrate the effectiveness of RHL-Net in harnessing RIS technology and the advanced spatial modeling of KAN for precise localisation, outperforming state-of-the-art methods on the evaluated dataset.

1. Introduction

The evolution of wireless communication has emerged in the era of next-generation wireless networks (NGWN), driven by the advancements in fifth-generation (5G) and emerging sixth-generation (6G) technologies, which aim to enhance connectivity, capacity, and intelligence in modern communication systems [1]. These networks harness the capabilities of high-frequency signals in the millimeter-wave (mmWave) and sub-millimeter wave spectrum to not only provide lightning-fast data transmission but also offer enhanced localisation solutions [2]. Precise localisation, defining a user device's exact location within a designated area, is paramount for maximising network efficiency, improving user satisfaction, and strengthening security measures [3]. Effective localisation also plays a crucial role in optimising radio and energy resource management and is essential for a range of applications, including asset tracking, spatial analytics, and immersive augmented/virtual reality AR/VR experiences.

Global navigation satellite systems (GNSS), such as GPS and GLONASS, provide widespread positioning services; however, their accuracy significantly deteriorates in challenging environments where satellite signals are obstructed [4]. These limitations are particularly evident in indoor settings, underground facilities, and dense urban landscapes with high-rise buildings, which cause signal attenuation, multipath interference, and non-line-of-sight (NLoS) conditions [5]. As a result, conventional GNSS-based localisation becomes unreliable, necessitating the development of alternative positioning solutions that can operate effectively in such constrained environments [6]. Moreover, relying on signals from multiple satellites can lead to increased energy consumption and latency issues, limiting their utility for certain applications [7]. In response to these challenges, researchers have directed significant efforts toward developing alternative localisation strategies tailored for indoor settings where GNSS performance is inadequate.

Innovations in localisation techniques have resulted in a spectrum of heuristic and AI-driven approaches that aim to enhance indoor positioning capabilities. Generally, these methods can be classified into active and passive localisation strategies [8]. Active localisation relies on the target device sending or responding to signals, thus achieving improved accuracy and control in the positioning process. On the other hand, passive localisation uses reflections and interactions of ambient signals, enabling non-invasive tracking, although often at the cost of reduced accuracy due to interference from environmental factors. This study focuses on the potential of active localisation methods, particularly those enhanced by reconfigurable intelligent surfaces (RIS) technology. RIS enables the adaptive manipulation of radio signals, which enhances their strength and mitigates the challenges posed by multipath fading, one of the significant barriers to accurate localisation [9]. By improving signal propagation characteristics, RIS offers a transformative solution to enhance localisation accuracy, especially in complex indoor settings where conventional methods yield poor localisation performance. Fig. 1 illustrates the system architecture of different RIS-assisted ad-hoc networks.

Localisation techniques can be divided into geometric algorithms and signal strength correlation methods. Geometric approaches-such as time-of-arrival (ToA), time-difference-of-arrival (TDoA), and angle-of-arrival (AoA) rely on precise measurements of signal timing or angles from multiple base stations for location estimation [10]. Although these methods can achieve remarkable precision, they often require strict time synchronisation, posing practical implementation challenges [11]. Conversely, signal strength correlation methods, including position fingerprinting, match the received signal strengths with pre-existing radio maps. While this approach is typically more cost-effective and eliminates the need for base station localisation, it can be time-intensive and vulnerable to inaccuracies stemming from environmental variability. Within the realm of fingerprinting techniques, channel state information (CSI)-based and received signal strength indicator (RSSI)-based methods have garnered attention. CSI captures intricate multipath information, including both amplitude and phase variations across frequencies, whereas RSSI focuses solely on signal strength. Both

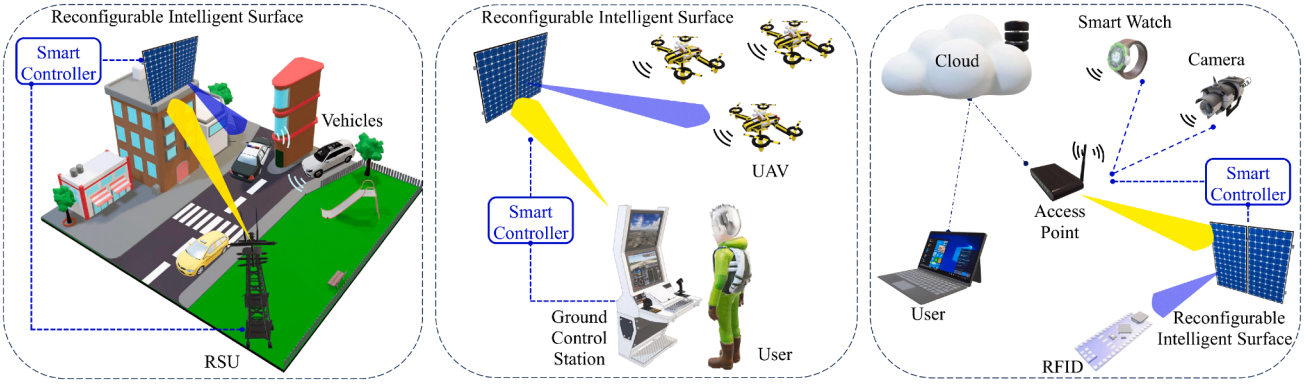

(a) RIS-assisted vehicular ad hoc networks. (b) RIS-assisted flying ad hoc networks. (c) RIS-assisted wireless sensor networks.

Fig. 1. The system architecture of various RIS-assisted ad hoc networks.

techniques involve an offline training phase to develop a signal map of the environment, followed by an online phase for user location estimation. However, both methodologies can suffer from the detrimental effects of multipath fading and signal degradation [12].

The introduction of RIS technology marks a significant advancement in addressing these challenges by enabling dynamic control over signal propagation, thereby optimising parameters such as amplitude, phase, and polarisation [13]. This capability helps to counteract the adverse impacts of multipath fading and boosts the performance of both CSI- and RSSI-based fingerprinting methods [14]. Consequently, RIS has the potential to redefine NGWN localisation, providing enhanced positioning accuracy without necessitating additional infrastructure investments. Despite the promising results of RIS technology in simulation studies, real-world applications remain largely uncharted. Initial investigations suggest that RIS can achieve sub-meter accuracy even in demanding environments, highlighting its potential to revolutionise localisation in scenarios where traditional systems falter. Additionally, the formulation and optimisation of novel machine learning models aimed at improving localisation accuracy is a vital aspect of ensuring reliable operational performance.

The proposed RIS-enhanced hybrid localisation network (RHL-Net) framework leverages RIS to elevate localisation accuracy through sophisticated signal processing techniques. It integrates long short-term memory (LSTM) networks [15] for temporal data analysis alongside Kolmogorov-Arnold networks (KAN) [16] for extracting spatial features. By utilising universal serial radio peripheral (USRP) transmitters and receivers, RHL-Net gathers signal data-including received signal strength (RSS) and channel phase response (θ)-from dual antennas spaced by different distances $x = \{0.5, 1\}$ meter apart. This arrangement allows the system to capture rich temporal and spatial features, facilitating accurate localisation. Through the synergistic integration of LSTM's temporal pattern recognition strengths and KAN's spatial dependency learning capabilities, RHL-Net addresses the challenges of signal propagation in RIS-augmented environments, significantly improving localisation accuracy for practical applications. The following summarises the contributions of this paper:

1. *Hybrid architecture*: RHL-Net effectively combines LSTM and KAN to enhance localisation accuracy by adeptly processing both sequential and spatial data within RIS environments. Incorporating LSTM networks effectively captures long-range dependencies and temporal patterns in signal data, surpassing the limitations of traditional recurrent networks.
2. *Spatial feature extraction with KAN*: KAN layers focus on learning spatial dependencies from received signals, thereby enhancing localisation accuracy through complex nonlinear function approximation. Regularisation techniques within KAN layers further bolster model generalisation, ensuring robust performance across diverse scenarios.
3. *Performance improvement*: RHL-Net achieves higher localisation accuracy than existing methods, demonstrating its effectiveness in real-world applications and supporting further advancements in RIS-based localisation technologies.

The remainder of this paper is structured as follows: Section 2 provides a review of the current state-of-the-art. Section 3 presents a detailed discussion of the proposed RHL-Net framework. Section 4 assesses the performance of the proposed approach through experimental analysis. Finally, Section 5 summarises this work.

2. Related work

Indoor localisation techniques have been extensively explored to mitigate the limitations of GNSS in obstructed environments. These methods, including ToA, TDoA, AoA, and RSSI, can be broadly classified into active and passive approaches. Active localisation requires direct signal exchange between the target device and infrastructure, ensuring higher accuracy and reliability. In contrast, passive localisation relies on analysing ambient RF signal reflections, making it less intrusive but more vulnerable to interference from obstacles, multipath effects, and dynamic environmental changes [17]. Within active localisation methods, RF-based techniques can be further classified into range-based and range-free approaches. Range-based systems use geometric mapping techniques like trilateration and triangulation, relying on estimating distances or angles from measured parameters such as RSSI, ToA, TDoA, and AoA. These techniques typically require multiple access points (APs) and are sensitive to multipath effects in complex environments [18]. On the other hand, range-free systems, such as fingerprinting, match measured signal parameters like RSSI and CSI to pre-existing databases to estimate location. Fingerprinting can operate effectively with a single AP in both LoS and NLoS environments but remains susceptible to challenges like multipath fading and environmental variability. Despite advancements in these methods, challenges such as high deployment costs, multipath fading, and environmental variability persist, affecting localisation accuracy and practicality.

In this challenging scenario, recent studies have proposed methods to reduce the number of required reference points (RPs) while maintaining localisation accuracy. In Moghtadaiee et al. [19], a zone-based path-loss model and a weighted ring-based interpolation technique are proposed to reconstruct RSS databases using fewer RPs. This approach reduces the number of required RPs by up to 89%, while achieving a $26-40\%$ improvement in localisation accuracy compared to conventional fingerprinting methods. In Guan et al. [20], a scalable and cost-effective system named "REAL" is introduced, which uses an adaptive RSS propagation model to reduce the need for extensive training data in large indoor environments. REAL incorporates a density-based clustering method for robust location estimation and is designed to function effectively even with sparse AP coverage. The system's adaptive model calibration makes it particularly suitable for large-scale deployments, offering improved accuracy over existing methods while requiring fewer training resources.

The authors in [21] propose a virtual fingerprint construction scheme (VFCS) to further minimise the labour-intensive offline phase of fingerprinting. VFCS uses a log-distance path loss model and interpolation methods to generate virtual RPs from a smaller set of real RPs, significantly reducing the need for extensive RSS measurements. To enhance the accuracy of this approach, a zone-based remedy algorithm is introduced, which refines location estimates by narrowing down the probable zone of the target. Experimental

Table 1
Comparison of indoor localisation techniques and RIS-assisted approaches.

Ref.	Method	Key Features	Accuracy	Limitations
[19]	Zone-based path-loss model	Reduces RPs by 89 %, improves RSS database	26–40 % better than conventional methods	Requires pre-existing RPs
[20]	Adaptive RSS model (REAL)	Uses clustering for robust localisation	Fewer training data, better accuracy	Depends on environment-specific signals
[21]	Virtual fingerprinting (VFCS)	Generates virtual RPs via interpolation	Reduces error to 1.25m	Requires initial real RPs
[22]	RIS-assisted mmWave MIMO	Iterative phase tuning	MSE: $> 10^{2}$m to $\sim 10^{-1}$m (−30 dB to 5 dB SNR)	Needs phase optimisation
[23]	Multi-user 3D RIS positioning	Low-complexity ToA-based RIS phase control	PEB < 1m	Assumes RIS-enabled users
[24]	RIS-aided 3D localisation	Evaluates synchronous/asynchronous effects	PEB of 8×10^{-4}m at 28 GHz	No real-world tests
[25]	RIS-based HW impairment mitigation	Uses multiple RISs, FIM analysis	PEB drops from 0.3m to 0.15m	Needs multiple RISs
[26]	RIS-enabled near-field positioning	Iterative phase optimisation	CRLB: 1m (−20 dB SNR) to <0.1m (20 dB SNR)	Requires precise RIS tuning
[27]	RIS for non-LoS localisation	Reshapes impulse responses	Improves non-LoS positioning	Needs hardware calibration
[28]	Reflection coefficient tuning	Pre-characterised lookup table	PEB: 10^{-3}m to 10^{-1}m (2-16m)	Degrades with distance
[29]	Experimental RIS indoor localisation	SVM/k-NN for classification	82.4 % accuracy, error <0.5m	Limited real-world generalisation
[30]	Dual-polarised RIS tracking	CNN-based moving target detection	BER: 10^{-5}, stable tracking	Requires CNN training

results show that VFCS combined with the zone-based remedy algorithm reduces average location estimation errors to around 1.25m in large indoor spaces, making it a viable solution for scalable indoor localisation with reduced time and cost. In Zhang et al. [22], the quality of fingerprints is further enhanced by incorporating the path-loss exponent (PLe) alongside RSSI values during fingerprint construction. This approach improves positioning precision by better capturing environmental characteristics while increasing robustness in resource-constrained environments.

Table 1 provides a comparative summary of indoor localisation techniques and RIS-assisted approaches. For instance, a multi-user 3D passive positioning approach using user equipment equipped with RIS is proposed in [23]. This study introduces a low-complexity ToA analysis algorithm that uses orthogonal sequences in RIS phase profiles for accurate localisation, aiming to minimise interference in passive systems where RIS is not part of the fixed infrastructure. Simulation results show that the proposed method achieves localisation errors close to the theoretical Cramér-Rao lower bounds (CRLB), reaching a positioning error bound (PEB) of less than 1 meter near the transmitter. Similarly, Elzanaty et al. [24] investigates RIS's role in next-generation wireless networks for improving user equipment localisation. The proposed architecture leverages RIS to aid in both position and orientation estimation at the gNB, utilising multiple antennas with 3D beamforming capabilities. This general model addresses both near-field and far-field localisation challenges in 3D space and examines the effects of synchronous and asynchronous signalling on localisation error. Through CRLB-based evaluations, the study demonstrates high accuracy, achieving a PEB of up to 8×10^{-4} meters at 28 GHz. In asynchronous scenarios, the proposed phase design closely approximates the optimal phase configuration, further reducing the CRLB.

In a related effort, Ghaseminajm et al. [25] explores the impact of hardware impairments (HWIs) on RIS-enhanced localisation in NGWNs. This work uses multiple RISs to counteract the detrimental effects of HWIs on localisation accuracy, providing an in-depth analysis of the Fisher information matrix (FIM) and implementing a robust maximum likelihood estimator (MLE). The study highlights the importance of RIS configuration and element count in improving localisation performance under HWI conditions. Notably, it is observed that as hardware imperfections decrease, the PEB improves from approximately 0.3 meters to under 0.15 meters across different inter-RIS spacings. Other studies have explored the potential of RIS for enhancing localisation in challenging conditions. For example, Luan et al. [26] investigates RIS-enabled near-field localisation in environments with obstructed line-of-sight (LoS) conditions. It presents a framework for optimising the RIS phase matrix to improve average localisation accuracy, employing a discretisation method and iterative entropy regularisation algorithm. Results show that the method significantly enhances CRLB, reducing it from around 1 meter at −20 dB SNR to below 0.1 meters at 20 dB SNR.

Additionally, research has shown RIS's effectiveness in rich scattering environments. In contrast to typical simulations that assume generic scattering, Alexandropoulos et al. [27] experimentally demonstrates RIS's ability to reshape channel impulse responses, thus enhancing communication rates and enabling precise non-LoS localisation of non-cooperative objects. Meanwhile, Rahal et al. [28] addresses the challenges posed by hardware constraints in RIS-based systems. By employing a pre-characterised lookup table of reflection coefficients, the study evaluates the effects of hardware limitations on beam power and secondary lobes, which influence localisation accuracy in non-LoS scenarios. Results indicate that the proposed method's PEB increases from below 10^{-3} meters to approximately 10^{-1} meters as the distance between the RIS and user equipment extends from 2 to 16 meters. The authors in [21] propose a dual-polarized RIS system that combines wireless communication and target tracking using a pre-trained artificial neural network (ANN). Convolutional neural networks (CNNs) and computer vision techniques enable the automatic detection of moving targets, leading to more intelligent wireless networks. The approach maintains reliable network coverage and achieves a stable bit error rate (BER) of 10^{-5} while tracking moving objects.

RIS has also been explored for applications in mmWave technologies. In [22], Jiguang et al. study RIS-assisted mmWave MIMO systems for joint localisation and communication, proposing an adaptive phase shifter design based on hierarchical codebooks and limited feedback. The method iteratively refines the combining vector at the mobile station, reducing the mean squared error (MSE) for position estimation from over 10^2 meters to around 10^{-1} meters as the SNR increases from -30 dB to 5 dB. Similarly, Rahal et al. [31] validates RIS-aided mmWave indoor positioning through a frequency-domain channel sounding campaign. The study assesses how RIS-reflected components like delay, AoA, and AoD affect positioning accuracy, highlighting practical challenges such as grating lobes and distance constraints. Results reveal a range of positioning errors, with median values as low as 0.07 meters and root mean squared rrrors (RMSE) reaching up to 3.22 meters.

The study in [29] conducts a detailed experimental analysis of RIS-enabled indoor localisation, utilising a dataset collected through an experimental setup with a 1-bit RIS panel consisting of 64×64 elements. The authors investigate the impact of RIS configurations, such as different antenna types, subcarrier settings, and communication modes, on localisation accuracy in an indoor environment. To achieve this, they employ machine learning algorithms, including support vector machines (SVM) and k-nearest neighbors (k-NN), for classification and regression tasks, aiming to predict the user's location. The experiments are conducted in a controlled indoor environment with varying RIS configurations, focusing on scenarios such as changing the angle of the RIS panel, adjusting the placement of antennas, and testing different subcarrier frequencies. The study evaluates the performance of each setup by measuring localisation accuracy, robustness, and the ability to handle NLoS conditions (i.e., low SNR values). Results from the study show that RIS significantly enhances localisation accuracy, achieving an 82.4% success rate in identifying the correct location class when using SVM, and reducing the mean localisation error to below 0.5 meters in some scenarios. However, despite these advancements, there remains a need for approaches that can further improve localisation accuracy while effectively addressing the challenges of signal propagation in complex indoor environments. By simulating low-SNR conditions, our experimental setup effectively represents longer-range and more challenging scenarios, demonstrating that RHL-Net combined with RIS maintains accurate localisation even under such conditions, while the framework's design supports generalization to larger and more complex environments.

3. The proposed framework

The proposed framework, RHL-Net, is a novel approach designed to enhance localisation accuracy by leveraging the capabilities of the RIS technology in conjunction with advanced signal processing techniques. The framework integrates sequential and spatial data analysis through the use of LSTM networks and KAN. Utilising USRP as a transmitter (Tx) and receiver (Rx) with single and multiple antennas, respectively, the system collects comprehensive signal data, including RSS and channel phase response, across a grid of different positions with interspacing distances $x = \{0.5, 1\}$ meter. This dual-channel setup provides rich feature sets for each position, capturing both the temporal dynamics and spatial variations influenced by the RIS. The RHL-Net framework processes this data through its hybrid architecture, combining the temporal pattern recognition of LSTM with the spatial feature extraction capabilities of KAN, to achieve robust and accurate localisation. KAN offers significant advantages, including the ability to approximate complex nonlinear functions and provide powerful generalization capabilities, making them particularly suited for capturing complex spatial dependencies in signal data. This approach aims to address the challenges of signal propagation and positioning in RIS-augmented communication systems, offering significant improvements in practical deployment scenarios. The following subsections present LSTM and KAN as fundamental components for extracting temporal features and capturing spatial dependencies, respectively.

3.1. The LSTM stage

LSTM network represents a significant advancement in recurrent neural networks (RNNs), particularly suited for tasks involving sequential data. Widely applied in domains such as sequence modeling, signal processing, and time series forecasting [32], LSTM networks address and resolve the limitations associated with traditional RNNs, notably the vanishing gradient problem. This makes them especially effective for learning and retaining long-term dependencies. This study uses LSTM to process the time-series data from the orthogonal frequency division multiplexing system with a number of N subcarriers. The LSTM module processes this data, capturing the temporal dependencies and patterns crucial for understanding signal propagation dynamics, especially with the influence of RIS which dynamically alters signal paths. An LSTM unit maintains two essential components at each time step t: the hidden state h_t and the cell state c_t. These components allow the LSTM to manage and propagate information over extended sequences. The architecture of an LSTM cell is distinguished by several gates that control the flow of information:

- *Forget gate* (f_t): Determines which parts of the cell state from the previous time step (c_{t-1}) are discarded.
- *Input gate* (i_t): Regulates the amount of new information added to the cell state.
- *Output gate* (o_t): Controls what part of the cell state is output to the next hidden state (h_t).
- *Cell candidate* ($\tilde{c}_t$): Represents the new candidate values that could be added to the cell state.

The mathematical expressions for these gates are given below, where σ is the sigmoid function, $\tanh$ is the hyperbolic tangent function, and W and b denote the weights and biases:

$$f_t = \sigma(W_f \cdot [h_{t-1}, x_t] + b_f) \tag{1a}$$

$$i_t = \sigma(W_i \cdot [h_{t-1}, x_t] + b_i) \tag{1b}$$

$$\tilde{c}_t = \tanh(W_c \cdot [h_{t-1}, x_t] + b_c) \tag{1c}$$

$$o_t = \sigma(W_o \cdot [h_{t-1}, x_t] + b_o) \tag{1d}$$

$$c_t = f_t \cdot c_{t-1} + i_t \cdot \tilde{c}_t \tag{1e}$$

$$h_t = o_t \cdot \tanh(c_t) \tag{1f}$$

By leveraging this gating mechanism, LSTMs effectively capture long-range dependencies and provide robust solutions for various sequential learning problems [33].

3.2. The Kolmogorov-Arnold stage

At this stage, we included this stage as a parallel processing unit to acquire and learn the spatial distribution of signal characteristics. The spatial data includes RSS and θ, capturing positional attributes and variations in signal quality across different locations. By analysing these spatial features, the KAN layers can effectively learn the spatial dependencies and contribute to precise localisation. The KAN is introduced as a novel neural network architecture inspired by the Kolmogorov-Arnold representation theorem. This approach offers a significant advancement over traditional multi-layer perceptrons (MLPs) by employing learnable activation functions on edges instead of fixed functions on nodes, leading to superior accuracy and interoperability.

In terms of architecture, KANs are fully-connected networks where each weight parameter is replaced by a learnable univariate function, typically parameterised as a spline. This architecture eliminates the need for linear weights, resulting in a network that sums incoming signals at nodes without applying non-linearities directly at the nodes. The use of splines as activation functions allows for flexible and accurate approximation of low-dimensional functions, and these splines can switch between coarse-grained and fine-grained grids, enhancing the model's adaptability and precision. The network operates by decomposing the high-dimensional function into a composition of univariate functions and summation operations, as shown in the Kolmogorov-Arnold representation:

$$f(x_1, \ldots, x_n) = \sum_{q=1}^{2n+1} \Phi_q \left(\sum_{p=1}^{n} \phi_{q,p}(x_p) \right) \tag{2}$$

A KAN layer can be defined as a matrix of 1D functions:

$$\Phi = \{\phi_{q,p}\}, \quad p = 1, 2, \ldots, n_{\text{in}}, \quad q = 1, 2, \ldots, n_{\text{out}} \tag{3}$$

where each $\phi_{q,p}$ function has trainable parameters, often represented as a combination of B-splines. The network's forward pass through a KAN layer is expressed as:

$$x_{l+1,j} = \sum_{i=1}^{n_l} \phi_{l,j,i}(x_{l,i}) \tag{4}$$

The B-spline basis functions $B_k(x)$, used to parametrise $\phi_{l,j,i}$, allow the network to finely adjust and optimise the activation functions. The overall activation function $\phi_{l,j,i}$ is a combination of a base activation function $b(x)$ and a spline function, providing residual connections similar to those in residual networks:

$$\phi_{l,j,i}(x) = w_b \cdot b(x) + w_s \cdot \sum_k c_k B_k(x) \tag{5}$$

The base activation function $b(x)$, typically a SiLU (Sigmoid linear unit) function defined as:

$$\text{SiLU}(x) = x \cdot \sigma(x) = \frac{x}{1 + e^{-x}} \tag{6}$$

It is combined with the spline function to offer both linear and nonlinear transformation capabilities. This structure allows KANs to approximate complex nonlinear functions efficiently, with faster scaling laws and improved generalization compared to traditional MLPs.

3.3. The proposed RHL-Net

The proposed RHL-Net integrates both LSTM networks and KAN to process sequential and spatial data for studying the effects of RIS on localisation. The data flow in RHL-Net begins with the LSTM module, which processes sequential data from the selected subcarriers in the OFDM system. The LSTM module has an input size of $(N/2 = 125, 4)$, a hidden size of 64, and consists of 2 layers, enabling it to capture complex temporal patterns. The output from the LSTM, reshaped into a flattened form, is then fed into a series of KAN layers. The KAN module operates in two branches: one processes the LSTM output while the other handles flattened spatial input data with a size of 500. Each KAN layer is designed with specific parameters: a grid size of 5, a spline order of 3, scale noise of 0.1, scale base of 1.0, scale spline of 1.0, and uses the SiLU as the base activation function. These parameters allow the KAN layers to flexibly and accurately approximate nonlinear functions through learnable B-spline functions. The grid epsilon is set to 0.02 to avoid numerical issues, and the grid range is defined from -1 to 1.

The features extracted from both KAN branches are concatenated and passed through a final classifier layer. This classifier takes the combined output and produces the final localisation output, identifying the position $(p_1 - p_9)$ with high accuracy. The RHL-Net also incorporates a regularization mechanism to control the activation magnitudes and entropy within the KAN layers, enhancing the generalization capabilities of the model. The overall architecture of the proposed model is shown in Fig. 2.

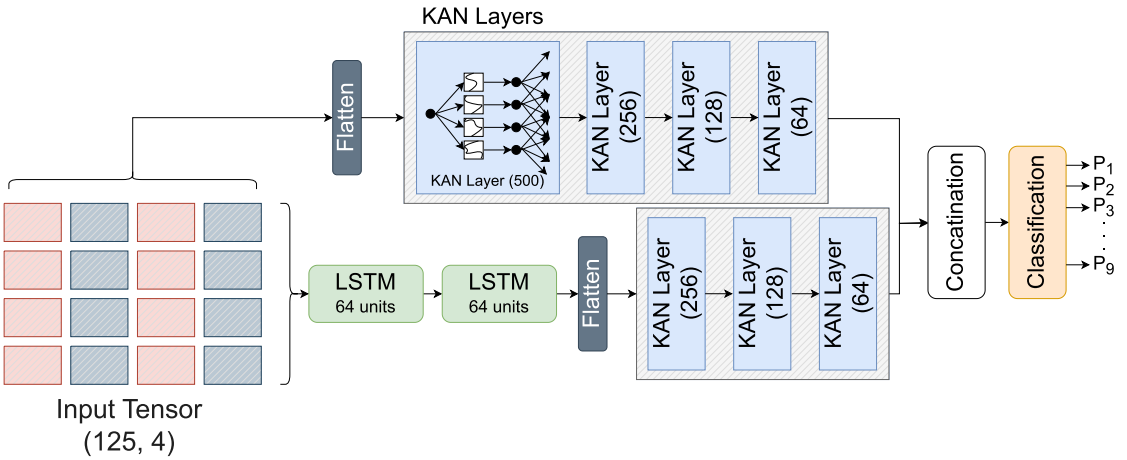

Fig. 2. The proposed RHL-Net model architecture. The classification task is multiclass, where each class corresponds to a discrete position ($P_1 - P_9$) within the environment. The model predicts the position class based on the input signal features from the OFDM system.

4. Results and discussion

In this section, we conducted multiple experiments to validate the performance of the proposed model, RHL-Net, including an ablation study of its components. Additionally, we compared the performance of RHL-Net under different configurations to assess the robustness of the model.

4.1. Experimental setup

To validate the practicality of the proposed method, the experiment was conducted in the Creativity Lab at the James Watt School of Engineering, University of Glasgow. The experimental configuration consists of a 1-bit RIS and two USRPs of model Ettus X300, serving as the Tx and Rx, see Fig. 3. The RIS employed in the experiment comprises 4096 elements, arranged in a 64×64 unit-cell structure and further segmented into 16 subarrays. Each subarray, measuring 33×33 cm^2, consists of 256 p-i-n diodes and a 16×16 unit-cell matrix. These unit cells are controlled through 16-bit LED drivers connected in a serial daisy chain configuration. The overall RIS prototype spans 132×132 cm^2 (equivalent to $16.5\lambda \times 16.5\lambda$ at 3.75 GHz) and is mounted on a 142×142 cm^2 polycarbonate sheet, which is affixed to an aluminium frame for structural stability. While a 1-bit RIS is used in this study, higher-resolution RIS, such as 4-bit devices, could reduce maximum phase quantization errors from 90° (1-bit) to 11.25° (4-bit), resulting in a more focused reflected beam, higher received signal strength, and potentially improving localisation accuracy under high multipath conditions. However, this improvement comes with significantly increased computational complexity. Specifically, a 64×64 RIS has 2^{4096} possible configurations with 1-bit resolution, whereas a 4-bit RIS has 16^{4096} configurations, making exhaustive optimisation infeasible. Additionally, RIS placement strongly influences localisation performance. In this study, the RIS was positioned to optimally reflect signals toward the receiver grid, maximizing coverage and signal reception.

To enable dynamic phase modulation, each subarray is equipped with five interface lines that facilitate voltage control, data transmission, and connectivity. The RIS control system is driven by a Raspberry Pi $3B+$, which manages data transfer through two SPI connections (SPI0 and SPI1) operating at 7.8 MHz. Communication between the MATLAB algorithm on a host PC and the Raspberry Pi is established via a WiFi link, where the Raspberry Pi functions as a hotspot to receive and process control commands. The transmitter and receiver employ Ettus X300 USRPs, which facilitate over-the-air signal transmission and reception. The transmitter is equipped with a single-directive antenna that features a 3 dB angular beamwidth of 80° in both the azimuth (E-plane) and elevation (H-plane). The receiver is tested with two antennas to implement a SIMO communication model. The dataset consists of channel measurements collected using a dual-channel USRP system and OFDM communication system, capturing both received signal strength and channel phase responses across a grid of spatial positions, enabling precise evaluation of localisation performance under various antenna configurations and RIS activation states.

The raw RSS and phase (θ) signals collected by the dual-channel USRP system were first preprocessed to reduce noise and improve signal quality. A bandpass filter was applied to remove out-of-band noise, followed by a moving average filter to smooth rapid fluctuations in the measurements. After preprocessing, the RSS and phase data were normalized using min-max scaling to map all values into the range $[0, 1]$, ensuring numerical stability and consistent input to the LSTM and RHL-Net models. Formally, for a signal x, the normalized value x_{norm} is computed as:

$$x_{\text{norm}} = \frac{x - x_{\min}}{x_{\max} - x_{\min}},$$

where $x_{\min}$ and $x_{\max}$ denote the minimum and maximum values of the signal, respectively. This preprocessing workflow ensures that the models learn from clean, representative signal patterns while minimizing the impact of measurement noise.

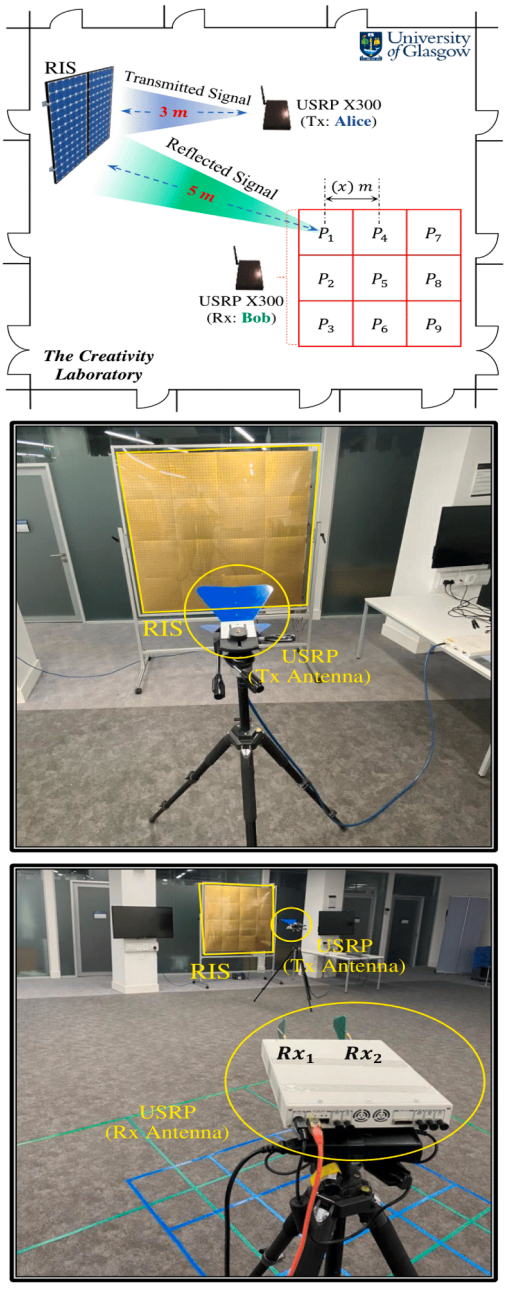

Fig. 3. The experimental setup.

To analyse the impact of antenna configurations on localisation accuracy, the experiment employs directional ultra-wideband (UWB) antennas at the receiver. More specifically, log-periodic directional antennas are used, covering a frequency range of 1.35 to 9.5 GHz, with a standing wave ratio below 2.5, directional linear polarisation, and a gain of $5-6$ dB. The experimental setup incorporates an OFDM-based communication system with $N = 256$ subcarriers and cyclic prefix lengths $CP = 64$. The carrier frequency is fixed at 3.75 GHz, while the sampling rate is set to 200 kHz. The OFDM signal structure is designed using LabVIEW, as shown in Fig. 4, where 105 subcarriers are allocated for zero-padding, 26 subcarriers are designated for channel probing and equalisation, 125 subcarriers are utilised for channel estimation, and 64 subcarriers are reserved for the CP. This configuration ensures that the LSTM input accurately reflects the relevant channel information for effective learning and localisation.

The data subcarriers are further employed for channel probing using reference symbols. The setup utilises the CBX-120 USRP daughterboard, which provides a bandwidth of up to 120 MHz for efficient signal processing. The experimental setup involves $T = 9$ receiver positions, with two distinct inter-position spacings of $x = \{0.5, 1\}$ m. The transmitter is placed 3 m away from the midpoint

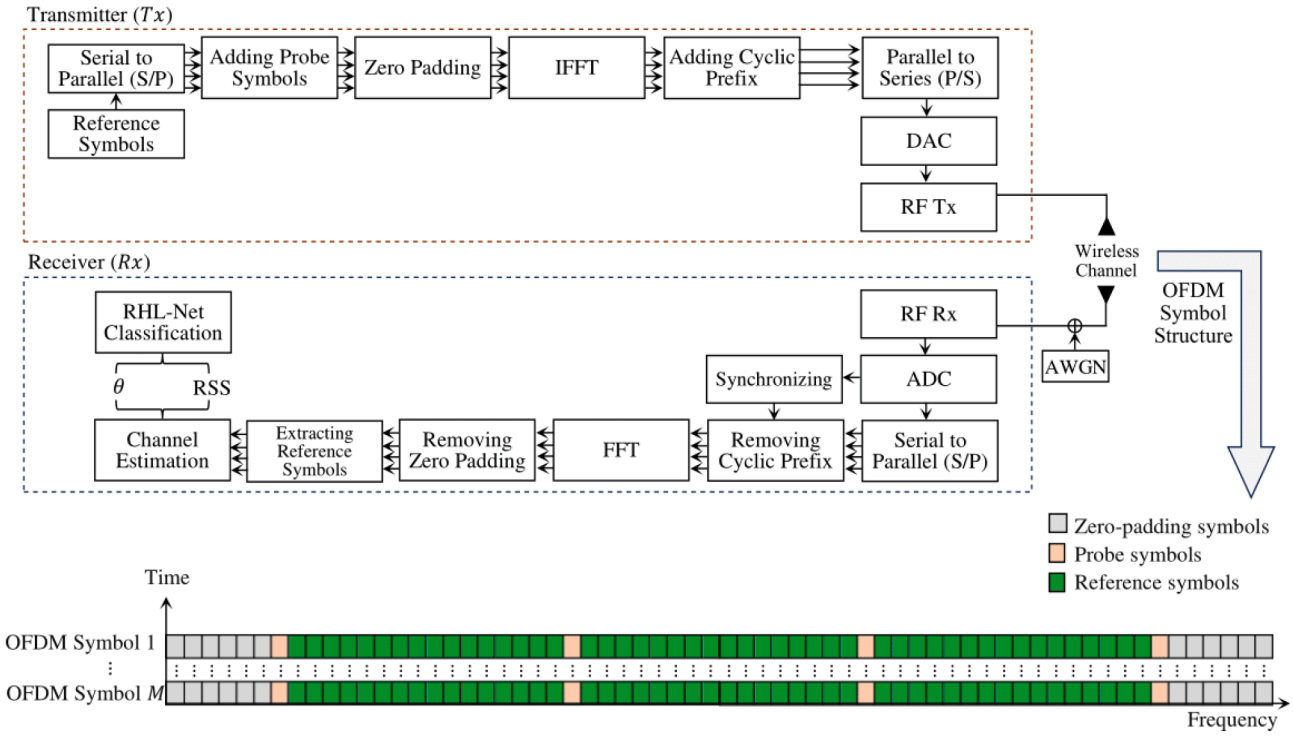

Fig. 4. Overview of the OFDM-based transmission and reception framework incorporating probe and reference symbols for enhanced channel estimation. The transmitter (Tx) processes data through serial-to-parallel conversion, probe symbol insertion, zero padding, IFFT, cyclic prefix addition, and RF transmission. The receiver (Rx) reconstructs the signal through RF reception, ADC conversion, synchronization, FFT, and cyclic prefix removal, followed by channel estimation and RHL-Net classification using received signal strength and channel phase response (θ). The OFDM symbol structure illustrates the distribution of zero-padding, probe, and reference symbols across time and frequency domains.

of the RIS, while the receiver at position 1 (P_1) is located at a distance of 5 m from the RIS. The transmitter antenna is positioned perpendicular to the RIS plane ($\theta_{\text{incident}} = 90°$), whereas the receiver antenna is oriented at $\theta_{\text{reflection}} = 135°$. Both antennas are mounted at a height of 126 cm, aligned with the midpoint of the RIS to ensure optimal reflection and reception.

4.2. Models configuration

The model configuration employed a deep neural network with hidden layers of sizes 256, 128, and 64, utilising the KAN architecture. The optimisation was performed using the Adam optimiser with a learning rate of 1×10^{-3} and a weight decay of 1×10^{-4}. A learning rate scheduler, ReduceLROnPlateau, was used to decrease the learning rate by a factor of 0.001 upon encountering a plateau in the loss minimisation, with a patience threshold of 10 epochs. An early stopping criterion with a patience of 20 epochs was applied to prevent overfitting. The experiments were conducted on a system equipped with an NVIDIA GeForce RTX 3090 GPU, utilizing the PyTorch framework, and ran for a maximum of 300 epochs.

4.3. Evaluation metrics

The performance of the proposed model is evaluated using standard classification metrics: Accuracy, Precision, Recall, and F1-Score. These metrics are derived from the counts of True Positives (TP), True Negatives (TN), False Positives (FP), and False Negatives (FN) across all classes. Their formal definitions are as follows:

$$\text{Accuracy} = \frac{TP + TN}{TP + TN + FP + FN}$$

$$\text{Precision} = \frac{TP}{TP + FP}$$

$$\text{Recall} = \frac{TP}{TP + FN}$$

$$\text{F1-Score} = 2 \times \frac{\text{Precision} \times \text{Recall}}{\text{Precision} + \text{Recall}}$$

For multi-class classification, these metrics are calculated globally by aggregging the counts of TP, TN, FP, and FN across all classes.

Table 2
Test accuracy and F1 Score for Models at 1 Meter and 0.5 Meter distances with directive and monopole antennas, with RIS activated and RIS deactivated.

Distance	Antenna Type	RIS Status	Model	Test Accuracy (%)	F1 Score (%)
0.5 Meter	Directive	Activated	LSTM	60.61	60.13
			Transformer	46.22	45.88
			MLP	61.06	60.71
		Deactivated	LSTM	50.72	50.89
			Transformer	34.44	31.38
			MLP	49.72	49.49
	Monopole	Activated	LSTM	67.78	67.21
			Transformer	48.56	48.95
			MLP	67.50	67.34
		Deactivated	LSTM	51.83	51.32
			Transformer	34.78	34.67
			MLP	46.56	45.98
1 Meter	Directive	Activated	LSTM	78.83	78.49
			Transformer	58.06	58.34
			MLP	77.72	77.35
		Deactivated	LSTM	61.22	61.43
			Transformer	42.00	42.28
			MLP	59.67	59.21
	Monopole	Activated	LSTM	68.06	68.23
			Transformer	53.78	52.09
			MLP	67.78	67.55
		Deactivated	LSTM	55.22	55.59
			Transformer	46.28	47.08
			MLP	54.94	54.81

Table 3
Configuration of deep learning baseline models.

Model	Architecture Details	Optimiser	Batch Size
LSTM	2 LSTM layers with hidden size of 128 Linear layer (128)	Adam (lr = 0.001)	128
Transformer	Input embedding layer (128) 2 Transformer encoder layers with 8 heads Linear layer (128) Mean pooling after Transformer layers	Adam (lr = 0.001)	128
MLP	Input linear layer (512) Hidden linear layers (512 → 256) Output linear layer (256) ReLU activations between layers	Adam (lr = 0.001)	128
KAN	Stacked KANLinear layers KAN layers: 256 → 128 → 64 SiLU activation with spline-based interpolation	Adam (lr = 0.001)	128
LSTM-KAN	2 LSTM layers (hidden size = 64) Flattened output fed to stacked KANLinear layers KAN layers: 256 → 128 → 64 Linear layer (64)	Adam (lr = 0.001)	128

4.4. Experimental series 1: DL baselines

In this section, we conducted experiments to evaluate the performance of DL baseline models, including LSTM, Transformer, MLP, KAN, and LSTM-KAN. Table 2 presents a comprehensive comparison of test accuracy and F1 scores across different configurations, examining the effects of distance, antenna type, and RIS activation on model performance. These results provide valuable insights for selecting optimal model components and rationales for the proposed architecture. Table 3 lists the configurations of the DL baseline models.

Across both distances (0.5 and 1 m), models with RIS activated consistently outperform their deactivated counterparts, particularly at the 1-meter distance. For instance, with the Directive antenna at 1 m, the LSTM model achieves the highest accuracy and F1 score (78.83 % and 78.49 %, respectively) when RIS is activated, surpassing the deactivated scenario by over 17 %. Similarly, for the Monopole antenna, RIS activation at 1 m yields improved performance for all models, with LSTM achieving 68.06 % accuracy compared to 55.22 % in the deactivated case.

Table 4
Accuracy and standard deviation of KAN, LSTM-KAN, and RHL-Net models for directive and monopole antennas with RIS activated and deactivated at 0.5 and 1 meter distances.

Distance	Antenna Type	RIS Status	Model	Accuracy (%)	Std
0.5 Meter	Directive	Activated	KAN	68.71	0.0069
			LSTM-KAN	63.59	0.0072
			RHL-Net	69.00	0.0076
		Deactivated	KAN	57.79	0.0090
			LSTM-KAN	55.10	0.0093
			RHL-Net	57.82	0.0118
	Monopole	Activated	KAN	73.28	0.0090
			LSTM-KAN	69.43	0.0051
			RHL-Net	74.19	0.0061
		Deactivated	KAN	56.53	0.0025
			LSTM-KAN	53.81	0.0074
			RHL-Net	57.04	0.0080
1 Meter	Directive	Activated	KAN	84.27	0.0066
			LSTM-KAN	82.70	0.0049
			RHL-Net	85.58	0.0104
		Deactivated	KAN	66.72	0.0079
			LSTM-KAN	65.12	0.0084
			RHL-Net	67.46	0.0118
	Monopole	Activated	KAN	73.76	0.0063
			LSTM-KAN	73.27	0.0030
			RHL-Net	73.88	0.0090
		Deactivated	KAN	63.43	0.0087
			LSTM-KAN	61.29	0.0091
			RHL-Net	64.89	0.0092

The Directive antenna generally enhances model performance more than the Monopole antenna, especially at 1 m, where it yields higher accuracy and F1 scores across models with RIS activated. This indicates that the Directive configuration benefits more from increased distance with RIS activation. However, at 0.5 m, the performance gap between Directive and Monopole antennas narrows, particularly for the MLP model, where the difference between Directive and Monopole with RIS activated is minimal (61.06 % vs. 67.50 %). The larger precision fluctuations observed for Monopole antennas at 1-meter spacing are primarily due to the combined effects of antenna directivity and multipath interference. Monopole antennas capture signals from multiple directions, making them more susceptible to multipath-induced variations, whereas Directive antennas provide more focused reception, resulting in more stable localisation performance.

The Transformer model consistently shows lower accuracy and F1 scores compared to LSTM and MLP across all settings, highlighting its limitations in this experimental setup. Conversely, LSTM and MLP models demonstrate robustness, particularly with RIS activation and the Directive antenna, achieving the highest scores in most configurations. The results underscore the significant positive impact of RIS activation on model performance, particularly with the Directive antenna at 1 m, and demonstrate the superior stability of LSTM and MLP over Transformer in this context.

4.5. Experimental series 2: KAN-based models

In this section, we compare the performance of the developed RHL-Net model with the traditional KAN and LSTM-KAN. The comparison results are given in Table 4. The results represent the average score across five runs for each model, with random initialization in each run to ensure the stability and reliability of model performance.

The analysis of the results listed in Table 4 indicates a clear influence of RIS activation, antenna type, and distance on model performance. Across all methods (KAN, LSTM-KAN, and RHL-Net), RIS activation consistently improves classification accuracy, with higher accuracies observed at both 0.5 and 1-meter distances. Notably, the RHL-Net model achieves the highest accuracy in most configurations, especially at 1 m with the Directive antenna and RIS activated (85.58 %), underscoring its robustness in this setup.

The performance is also impacted by the antenna type, with the Monopole antenna showing improved accuracy over the Directive antenna in several cases, although the Directive antenna at 1 m with RIS activated yields the peak results for most models. This suggests that the Directive antenna, combined with RIS activation at greater distances, optimally enhances signal classification capabilities.

STD values complement the accuracy metrics, generally aligning with the accuracy trends and demonstrating reduced values when RIS is activated. This suggests that RIS activation not only improves classification accuracy but also stabilizes model predictions by reducing uncertainty. The lowest STD values are observed with the KAN model at 1 m with RIS activated, indicating efficient learning under these conditions. The results validate the benefit of RIS activation, particularly in conjunction with the Directive antenna at longer distances, enhancing the performance of all models, with RHL-Net exhibiting superior accuracy overall.

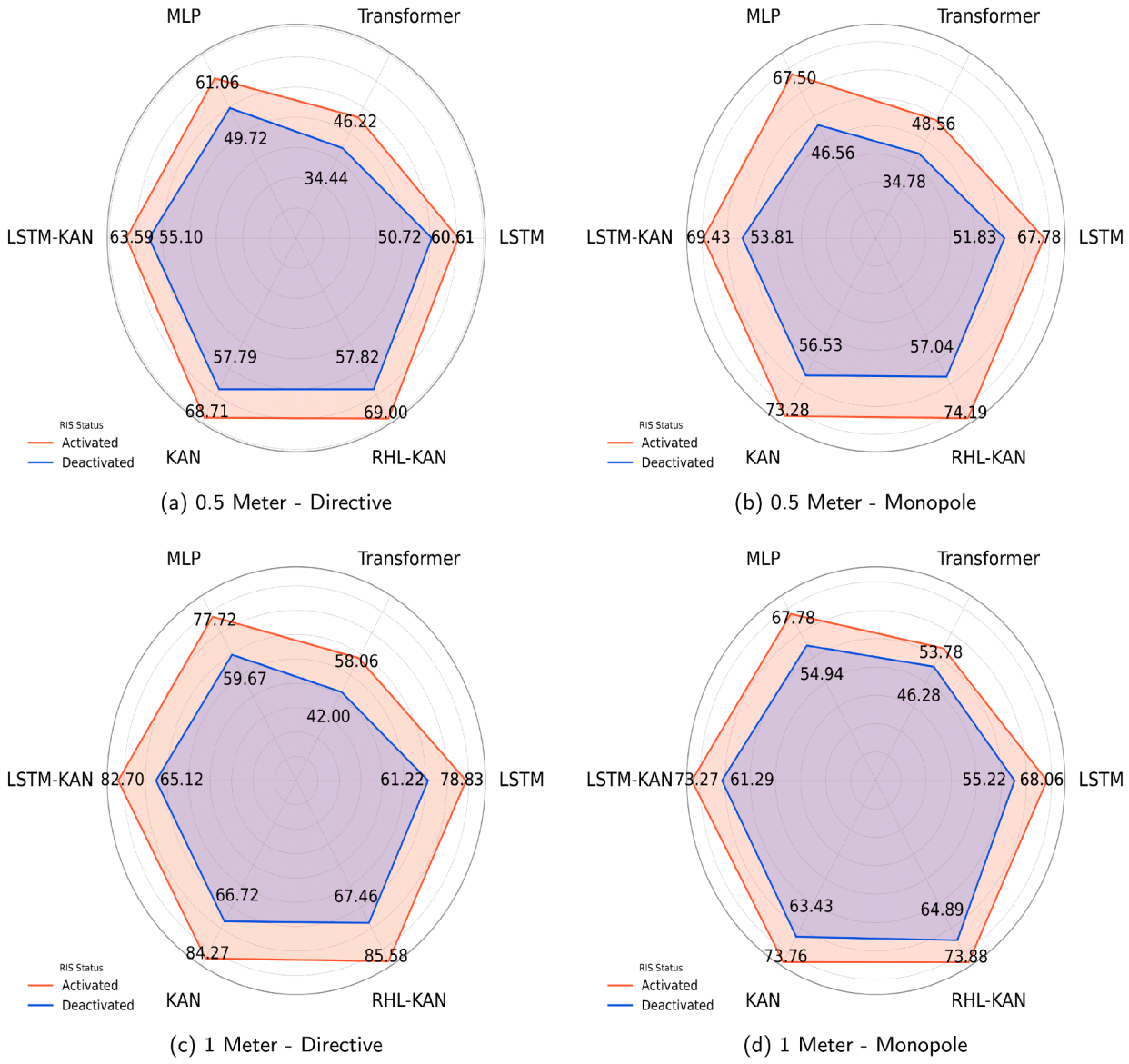

Fig. 5. The performance of various models using different configurations and models.

4.6. Experimental series 3: Configurations analysis

The charts in Fig. 5 for each configuration provide a comparative visual analysis of the performance of various models (LSTM, Transformer, MLP, LSTM-KAN, KAN, RHL-Net) under different conditions.

The charts in 5 indicate that activating the RIS significantly enhances model accuracy across most configurations, especially for architectures like RHL-Net and KAN. For instance, RHL-Net achieves an accuracy of up to 85.58 % in the 1m-Directive-Activated configuration, outperforming other models and highlighting its robustness in complex signal environments. In contrast, when RIS is deactivated, accuracy generally declines across models, with RHL-Net and KAN still outperforming others but showing a slight drop, such as RHL-Net's 67.46 % accuracy in the 1m-Directive-Deactivated configuration. This pattern underscores the critical role of RIS in enhancing signal quality for classification.

The Directive antenna configuration shows a consistent performance advantage over the Monopole antenna, particularly at a distance of 1 m. For example, KAN achieves an accuracy of 84.27 % with RIS activated at 1 m using the Directive antenna, whereas the same configuration with the Monopole antenna reaches only 73.76 %. This suggests that the focused signal of the Directive antenna may be better suited for capturing data patterns relevant to the classification task.

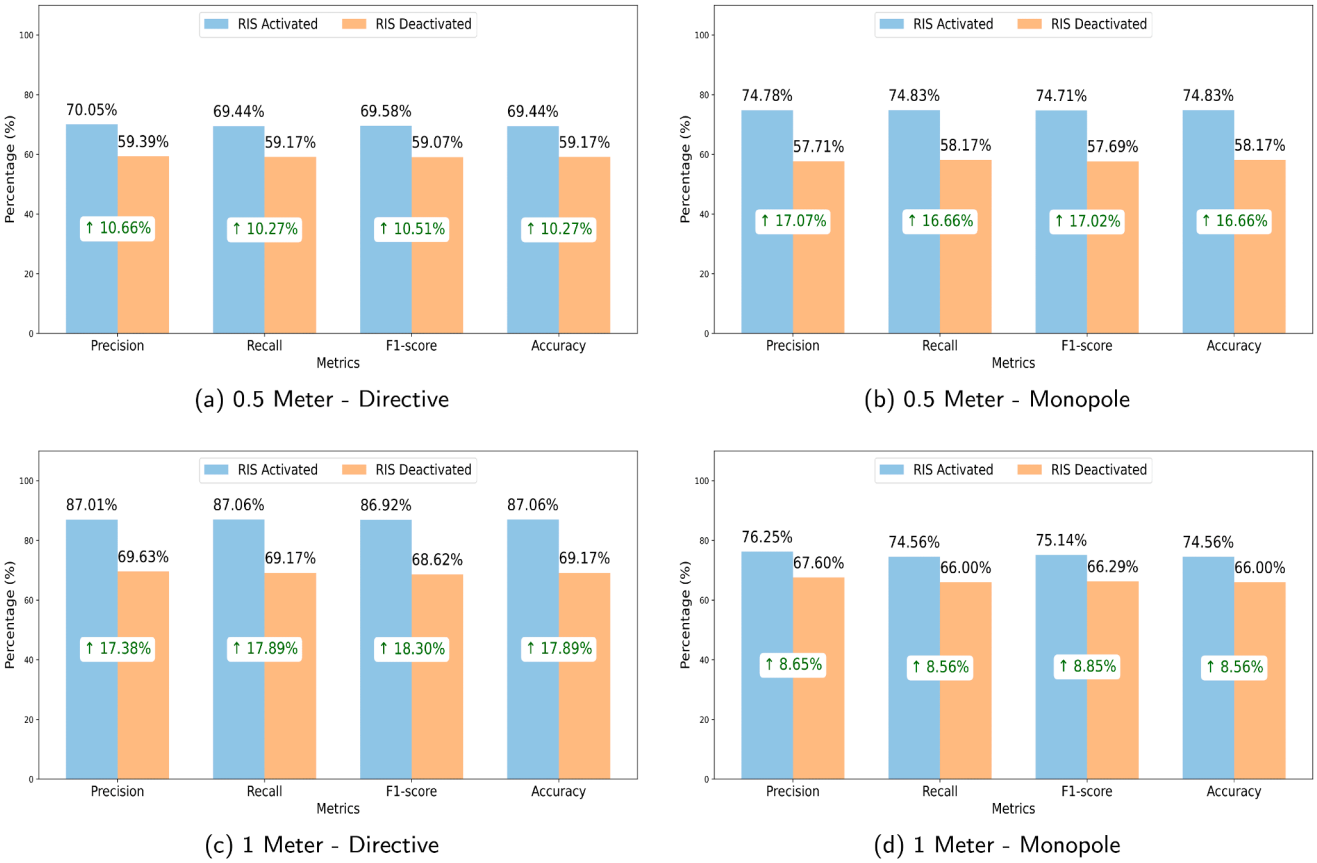

Fig. 6. The performance metrics of RHL-Net using different configurations.

Among the models, the simpler architectures like LSTM and MLP show increased variability and lower performance, especially in RIS-deactivated conditions. For example, the accuracy of LSTM drops to 61.22 % in the 1m-Directive-Deactivated configuration compared to 78.83 % when RIS is activated, highlighting a dependency on a stable signal environment. The Transformer model, while providing moderate results, consistently trails other models in accuracy, reaching only 58.06 % in the 1m-Directive-Activated configuration, suggesting it may be less adapted to the temporal and spatial dependencies of this specific data. In conclusion, RIS activation and the Directive antenna configuration significantly boost performance, with RHL-Net model leading in accuracy. These findings highlight the importance of RIS and antenna choice, which, combined with robust model architectures, can optimise signal-based classification tasks in challenging environments.

The bar charts in Fig. 6 provide a comparative analysis of four performance metrics, Precision, Recall, F1-score, and Accuracy, across different antenna types (Directive and Monopole) and distances (1 m and 0.5 m) for configurations with the RIS either Activated or Deactivated. The presented results are based on the performance of the best run using RHL-Net model on the described dataset.

For the 1 m Directive configuration, activation of RIS yields significant improvements across all metrics, with Precision, Recall, F1-score, and Accuracy values of 87.01 %, 87.06 %, 86.92 %, and 87.06 %, respectively, compared to the deactivated configuration values of 69.63 %, 69.17 %, 68.62 %, and 69.17 %. This represents an approximate 17 % improvement across the metrics. While the 1 m Monopole configuration shows a similar trend, though the increase is less pronounced. With RIS activated, Precision, Recall, F1-score, and Accuracy reach 76.25 %, 74.56 %, 75.14 %, and 74.56 %, respectively, compared to the deactivated configuration values of 67.60 %, 66.00 %, 66.29 %, and 66.00 %. This yields an approximate improvement of around 8 % in all metrics.

In the 0.5 m Directive setup, RIS activation again enhances performance, though the overall metric values are lower than the 1 m Directive configuration. The activated configuration achieves Precision, Recall, F1-score, and Accuracy values of 70.05 %, 69.44 %, 69.58 %, and 69.44 %, compared to 59.39 %, 59.17 %, 59.07 %, and 59.17 % for the deactivated configuration, showing an improvement of around 10 %. Finally, the 0.5-meter Monopole configuration shows similar performance gains with RIS activation, yielding Precision, Recall, F1-score, and Accuracy of 74.78 %, 74.83 %, 74.71 %, and 74.83 %, compared to 57.71 %, 58.17 %, 57.69 %, and 58.17 % for the deactivated setup, with an improvement of approximately 16 %.

Overall, the charts demonstrate that activating RIS consistently improves classification performance across all setups, with the largest gains observed in the 0.5 m Monopole configuration, suggesting that RIS activation has the most substantial impact when operating under these conditions.

Table 5
Comparison with State-of-the-Art (SOTA) models for directive and monopole antennas with RIS activated and deactivated at 0.5 and 1 meter distances.

Distance	Antenna Type	RIS Status	Method	Accuracy (%)	Std
0.5 Meter	Directive	Activated	GBT [29]	72.30	1.7
			RHL-Net	69.00	0.0076
		Deactivated	GBT	54.50	1.9
			RHL-Net	57.82	0.0118
	Monopole	Activated	GBT	68.80	1.7
			RHL-Net	74.19	0.0061
		Deactivated	GBT	51.40	1.9
			RHL-Net	57.04	0.0080
1 Meter	Directive	Activated	GBT	82.40	1.4
			RHL-Net	85.58	0.0104
		Deactivated	GBT	63.30	1.8
			RHL-Net	67.46	0.0118
	Monopole	Activated	GBT	69.80	1.7
			RHL-Net	73.88	0.0090
		Deactivated	GBT	59.40	1.8
			RHL-Net	64.89	0.0092

4.7. Experimental series 4: Inference time vs. accuracy trade-off analysis

The inference time versus accuracy trade-off was systematically evaluated across all experimental configurations, with the results summarized in Fig. 7. Several key patterns emerge from this comprehensive analysis.

4.7.1. Performance and efficiency trends

Across all configurations, a clear hierarchy in computational efficiency is observed. The pure KAN architecture consistently demonstrates superior inference speed, operating at approximately 0.022 seconds, which is 3× faster than LSTM-KAN (∼ 0.065 seconds) and 6× faster than the full RHL-Net (∼ 0.135 seconds). This efficiency advantage extends to training times, where KAN requires only 4.5–4.8 seconds compared to 30–67 seconds for the hybrid architectures.

Despite its computational efficiency, KAN maintains competitive accuracy across most scenarios. In the 0.5-meter Directive configuration with RIS, KAN achieves 68.71 % accuracy compared to RHL-Net's 69.00 %, while requiring only 8.8 % of the training time. Similarly, in the 1-meter Directive with RIS scenario, KAN attains 84.27 % versus RHL-Net's 85.58 %, representing a minimal 1.5 % performance gap for a substantial 92 % reduction in training time.

4.7.2. RIS impact on model efficiency

The presence of RIS significantly influences the accuracy-efficiency trade-off. In Directive antenna configurations with RIS activated, RHL-Net demonstrates its strongest performance advantage, achieving accuracy improvements of 11.2–18.1 percentage points over the no-RIS baseline. However, this performance comes at the cost of computational overhead, with RHL-Net requiring approximately 50–60 seconds of training time versus 4.5–4.8 seconds for KAN.

Notably, in Monopole configurations, the performance gap narrows considerably. For 1-meter Monopole with RIS, all three models achieve comparable accuracy (73.27 %–73.88 %), suggesting that in certain scenarios, the simpler KAN architecture may provide the most favorable efficiency-to-performance ratio.

The choice between architectures depends on application requirements. For latency-critical applications where near-real-time inference is essential, KAN provides the optimal balance with consistent sub-0.025-second inference times while maintaining competitive accuracy. For applications where maximum accuracy is paramount and computational resources are sufficient, RHL-Net offers performance advantages, particularly in challenging Directive antenna configurations with RIS enhancement.

The LSTM-KAN hybrid occupies an intermediate position, offering moderate improvements over pure KAN in some scenarios. This makes it suitable for applications requiring a balance between performance and computational constraints.

The parameter analysis reveals distinct computational footprints across the three architectures, with RHL-Net comprising the largest model at 22.6 million parameters, closely followed by LSTM-KAN at 20.9 million parameters. In contrast, the pure KAN architecture demonstrates remarkable parameter efficiency with only 1.7 million parameters.

4.8. Experimental series 5: Comparison with SOTA

In this section, we compare the performance of the developed RHL-Net model with other state-of-the-art methods. The results of the comparison are given in Table 5. The results demonstrate a clear improvement in accuracy for RHL-Net compared to Gradient Boosted Trees (GBT) [29] across all configurations, with RHL-Net outperforming GBT by notable margins. At 1 m with the Directive

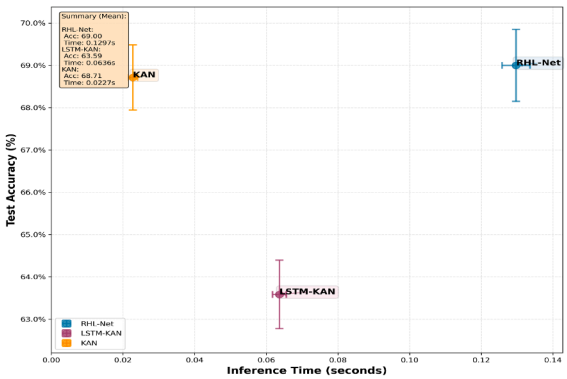

(a) 0.5 Meter - Directive (RIS Activated)

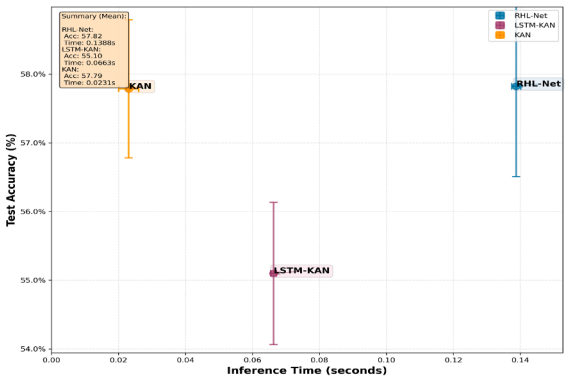

(b) 0.5 Meter - Directive (RIS Deactivated)

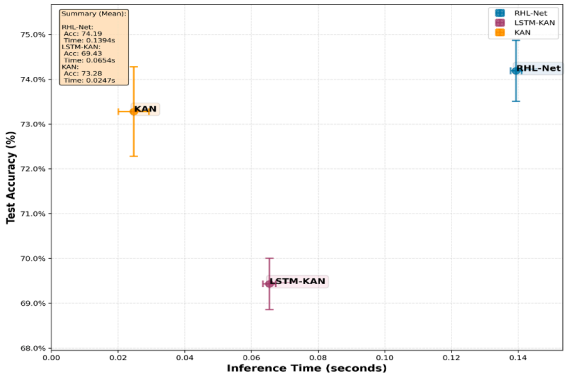

(c) 0.5 Meter - Monopole (RIS Activated)

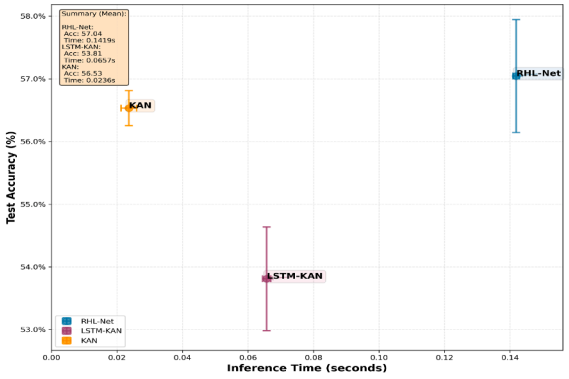

(d) 0.5 Meter - Monopole (RIS Deactivated)

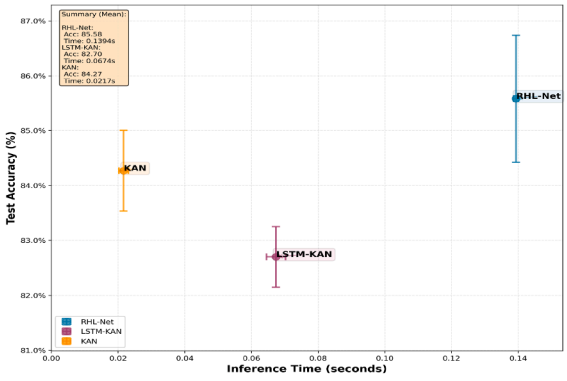

(e) 1 Meter - Directive (RIS Activated)

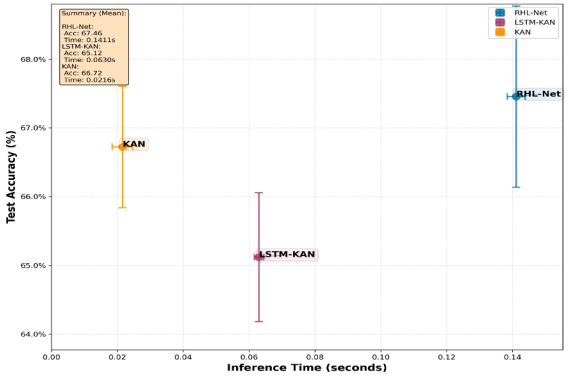

(f) 1 Meter - Directive (RIS Deactivated)

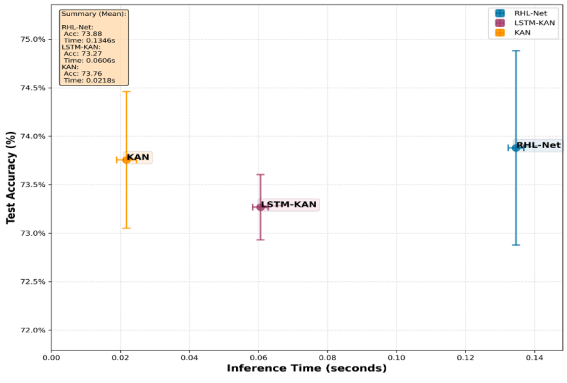

(g) 1 Meter - Monopole (RIS Activated)

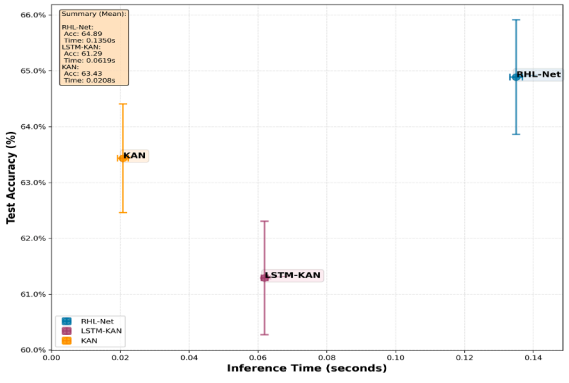

(h) 1 Meter - Monopole (RIS Deactivated)

Fig. 7. Inference time vs. Accuracy tradeoffs using different models.

antenna and RIS activated, RHL-Net achieves an accuracy of 85.58 %, marking a 3.18 % improvement over GBT's 82.40 %. Similarly, with the Monopole antenna under the same conditions, RHL-Net records an accuracy of 73.88 %, which is 4.08 % higher than GBT's 69.80 %.

At 0.5 m, RHL-Net also shows substantial gains. With the Directive antenna and RIS activated, RHL-Net attains an accuracy of 69.00 %, a 3.00 % improvement over GBT's 72.30 %. Likewise, in the Monopole antenna configuration, RHL-Net reaches 74.19 %, representing a 5.39 % increase over GBT's 68.80 %. These differences underscore the robustness of RHL-Net, particularly in RIS-activated environments, where it consistently achieves higher accuracy and demonstrates greater resilience to signal variations. The improvements indicate that RHL-Net can effectively leverage the added signal clarity from RIS activation, making it a superior choice for signal classification tasks compared to the traditional GBT model. We note that in the specific 0.5m Directive RIS-activated case, GBT slightly outperforms RHL-Net; however, across the majority of configurations and more challenging scenarios, RHL-Net maintains its superior performance, highlighting its generalization and robustness.

5. Conclusions and future trends

This study presents RHL-Net, a hybrid localisation framework that combines RIS with advanced deep learning architectures, effectively enhancing localisation accuracy. The integration of LSTM and KAN within RHL-Net enables the framework to simultaneously process sequential and spatial data, offering robust performance in challenging propagation environments. Experimental results demonstrate that RHL-Net (best run) significantly improves localisation accuracy across different setups, particularly with RIS activation. For instance, in the 1 m Directive configuration, the framework achieved a precision of 87.01 %, recall of 87.06 %, F1-score of 86.92 %, and accuracy of 87.06 % with RIS activated, compared to lower metrics in the deactivated scenario. Similarly, the 0.5 m Monopole configuration saw substantial gains, with RIS activation yielding a precision of 74.78 % and accuracy of 74.83 %, representing an approximate 16 % improvement over the deactivated configuration.

Experimental evaluations show that RHL-Net achieves substantial improvements in accuracy across various scenarios, demonstrating the efficacy of the framework in leveraging RIS-induced spatial variations for precise positioning. The dual-channel USRP setup, which collects RSS and phase response data, enhances feature richness, allowing RHL-Net to capture complex spatial dependencies. Future work will focus on optimising the architecture for different RIS configurations and expanding the applicability of the framework to diverse communication environments. Additionally, we plan to extend the current discrete classification approach to enable continuous position estimation in the real-time, which will allow the use of metrics such as mean absolute error and cumulative distribution error to further evaluate localisation performance.

Declaration

Declaration of generative AI and AI-assisted technologies in the writing process: During the preparation of this work the author(s) used Grammarly in order to improve the language and readability. After using this tool/service, the author(s) reviewed and edited the content as needed and take(s) full responsibility for the content of the publication.

CRediT authorship contribution statement

Abdelghani Dahou: Writing – original draft, Methodology, Investigation, Formal analysis, Conceptualization; **Syed Tariq Shah:** Writing – review & editing, Writing – original draft, Supervision, Resources, Formal analysis, Data curation, Conceptualization; **Insaf Ullah:** Visualization, Validation, Methodology, Formal analysis; **Tahira Mahboob:** Writing – review & editing, Visualization, Validation, Software, Formal analysis; **Ahmed Gamal Abdellatif:** Writing – review & editing, Validation, Software; **Mohamed Abd Elaziz:** Visualization, Investigation, Formal analysis; **Ahmad Almogren:** Writing – review & editing, Supervision, Project administration, Methodology, Funding acquisition; **Mahmoud A. Shawky:** Writing – review & editing, Writing – original draft, Validation, Investigation, Formal analysis, Data curation, Conceptualization.

Data availability

Data will be made available on request.

Declaration of competing interest

The authors declare that they have no known competing financial interests or personal relationships that could have appeared to influence the work reported in this paper.

Acknowledgment

This work was supported by King Saud University, Riyadh, Saudi Arabia through the Ongoing Research Funding program number ORF-2025-184.

References

[1] M.A. Shawky, S.T. Shah, M. Abdrabou, M. Usman, Q.H. Abbasi, D. Flynn, M.A. Imran, S. Ansari, How secure are our roads? An in-depth review of authentication in vehicular communications, Veh. Commun. 47 (2024) 100784. https://doi.org/10.1016/j.vehcom.2024.100784

[2] M.M. Ahmed, M.A. Shawky, S. Zahran, A. Moussa, N. El-Shimy, A.A. Elmahallawy, S. Ansari, S.T. Shah, A.G. Abdellatif, An experimental analysis of outdoor UAV localisation through diverse estimators and crowd-sensed data fusion, Phys. Commun. 66 (2024) 102475. https://doi.org/10.1016/j.phycom.2024.102475

[3] Q. Wu, R. Zhang, Towards smart and reconfigurable environment: intelligent reflecting surface aided wireless network, IEEE Commun. Mag. 58 (1) (2020) 106–112. https://doi.org/10.1109/MCOM.001.1900107

[4] K. Keykhosravi, A. Khalajmehrabadi, Y. Zhao, M. Win, Leveraging RIS-enabled smart signal propagation for solving infeasible localization problems: scenarios, key research directions, and open challenges, IEEE Veh. Technol. Mag. 18 (1) (2023) 20–28. https://doi.org/10.1109/MVT.2022.3223854

[5] M. Usman, J. Rains, T.J. Cui, Intelligent wireless walls for contactless in-home monitoring, Light Sci. Appl. 11 (2022) 212. https://doi.org/10.1038/s41377-022-00786-5

[6] A.A. Salama, M.A. Shawky, S.H. Darwish, A.A. Elmahallawy, M. Elaziz, A. Almogren, A.G. Abdellatif, S.T. Shah, Unlocking the dynamic potential: next-gen DOA estimation for moving signals via BSCS with adaptive weighted Kalman filter in 6G networks, Internet of Things 30 2025. https://doi.org/10.1016/j.iot.2024.101486

[7] Z. Farid, R. Nordin, M. Ismail, Recent advances in wireless indoor localization techniques and system, 2013, p. 185138. https://doi.org/10.1155/2013/185138

[8] F. Zafari, A. Gkelias, K.K. Leung, A survey of indoor localization systems and technologies, IEEE Commun. Surveys Tuts 21 (3) (2019) 2568–2599. https://doi.org/10.1109/COMST.2019.2911558

[9] M.A. Shawky, S.T. Shah, Q.H. Abbasi, M. Hussein, M.A. Imran, S.F. Hasan, S. Ansari, A. Taha, RIS-enabled secret key generation for secured vehicular communication in the presence of denial-of-service attacks, Sensors 23 (2023) 4104. https://doi.org/10.3390/s23084104

[10] H. Obeidat, W. Shuaieb, O. Obeidat, et al, A review of indoor localization techniques and wireless technologies, Wireless Pers. Commun. 119 (2021) 289–327. https://doi.org/10.1007/s11277-021-08209-5

[11] X. Zhu, Y. Shen, H. Zhou, R. He, B. Wang, Y. Chen, B. Ai, Z. Xu, Indoor intelligent fingerprint-based localization: principles, approaches and challenges, IEEE Commun. Surveys Tuts 22 (4) (2020) 2634–2657. https://doi.org/10.1109/COMST.2020.3014191

[12] P. Lazik, N. Rajagopal, B. Sinopoli, A. Rowe, Ultrasonic time synchronization and ranging on smartphones, in: Proc. 2015 IEEE Real-Time and Embedded Technology and Applications Symposium (RTAS), 2015 IEEE Real-Time and Embedded Technology and Applications Symposium (RTAS), 2015, pp. 108–118. https://doi.org/10.1109/RTAS.2015.7108422

[13] M. Stahlke, G. Yammine, T. Feigl, B.M. Eskofier, C. Mutschler, Indoor localization with robust global channel charting: a time-distance-based approach, IEEE Trans. Mach. Learn. Commun. Netw. 1 (2023) 3–17. https://doi.org/10.1109/TMLCN.2023.3274596

[14] K.M. Faisal, W. Choi, Machine learning approaches for reconfigurable intelligent surfaces: a survey, IEEE Access 10 (2022) 27343–27367. https://doi.org/10.1109/ACCESS.2022.3156737

[15] B. Lindemann, T. Müller, H. Vietz, N. Jazdi, M. Weyrich, A survey on long short-term memory networks for time series prediction, Procedia CIRP 99 (2021) 650–655. https://doi.org/10.1016/j.procir.2021.03.088

[16] Z. Liu, Y. Wang, S. Vaidya, F. Ruehle, J. Halverson, M. Soljačić, T.Y. Hou, M. Tegmark, KAN: Kolmogorov-Arnold Networks, arXiv:2404.19756, 2025.

[17] S.J. Hayward, K.V. Lopik, C. Hinde, A.A. West, A survey of indoor location technologies, techniques and applications in industry, Internet of Things 20 (2022) 100608. https://doi.org/10.1016/j.iot.2022.100608

[18] S. Shang, L. Wang, Overview of WiFi fingerprinting-based indoor positioning, IET Commun. 16 (7) (2022) 725–733.

[19] V. Moghtadaiee, S.A. Ghorashi, M. Ghavami, New reconstructed database for cost reduction in indoor fingerprinting localization, IEEE Access 7 (2019) 104462–104477. https://doi.org/10.1109/ACCESS.2019.2932024

[20] T. Guan, L. Fang, W. Dong, D. Koutsonikolas, G. Challen, C. Qiao, Robust, cost-effective and scalable localization in large indoor areas, Comput. Netw. 120 (2017) 43–55. https://doi.org/10.1016/j.comnet.2017.04.032

[21] Y.-H. Wu, Y.-L. Chen, S.-T. Sheu, Indoor location estimation using virtual fingerprint construction and zone-based remedy algorithm, in: Proc. 2016 Int. Conf. Commun. Problem-Solving, 2016 Int. Conf. Commun. Problem-Solving, 2016, pp. 1–3. https://doi.org/10.1109/ICCPS.2016.7751132

[22] J. Zhang, G. Han, N. Sun, L. Shu, Path-loss-based fingerprint localization approach for location-based services in indoor environments, IEEE Access 5 (2017) 13756–13769.

[23] K. Keykhosravi, M.F. Keskin, S. Dwivedi, G. Seco-Granados, H. Wymeersch, Semi-passive 3D positioning of multiple RIS-enabled users, IEEE Trans. Veh. Technol. 70 (10) (2021) 11073–11077. https://doi.org/10.1109/TVT.2021.3109786

[24] A. Elzanaty, A. Guerra, F. Guidi, M.-S. Alouini, Reconfigurable intelligent surfaces for localization: position and orientation error bounds, IEEE Trans. Signal Process. 69 (2021) 5386–5402. https://doi.org/10.1109/TSP.2021.3101644

[25] F. Ghaseminajm, M. Alsmadi, D. Tubail, S.S. Ikki, RIS-aided mobile localization error bounds under hardware impairments, IEEE Trans. Commun. 70 (12) (2022) 8331–8341. https://doi.org/10.1109/TCOMM.2022.3220319

[26] M. Luan, B. Wang, Y. Zhao, Z. Feng, F. Hu, Phase design and near-field target localization for RIS-assisted regional localization system, IEEE Trans. Veh. Technol. 71 (2) (2022) 1766–1777. https://doi.org/10.1109/TVT.2021.3135275

[27] G.C. Alexandropoulos, N. Shlezinger, P.D. Hougne, Reconfigurable intelligent surfaces for rich scattering wireless communications: recent experiments, challenges, and opportunities, IEEE Commun. Mag. 59 (6) (2021) 28–34. https://doi.org/10.1109/MCOM.001.2001117

[28] M. Rahal, B. Denis, K. Keykhosravi, M.F. Keskin, B. Uguen, G.C. Alexandropoulos, H. Wymeersch, Performance of RIS-aided near-field localization under beams approximation from real hardware characterization, EURASIP J. Wireless Commun. Netw. 2023 (1) (2023) 86. https://doi.org/10.1186/s13638-023-02294-9

[29] S.T. Shah, M.A. Shawky, J.U.R. Kazim, A. Taha, S. Ansari, S.F. Hasan, M.A. Imran, Q.H. Abbasi, Coded environments: data-driven indoor localisation with reconfigurable intelligent surfaces, Commun. Eng. 3 (1) (2024) 66.

[30] W. Li, Q. Ma, C. Liu, Y. Zhang, X. Wu, J. Wang, S. Gao, T. Qiu, T. Liu, Q. Xiao, J. Wei, T. Gu, Z. Zhou, F. Li, Q. Cheng, L. Li, W. Tang, T. Cui, Intelligent metasurface system for automatic tracking of moving targets and wireless communications based on computer vision, Nat. Commun. 14 (1) (2023) 989. https://doi.org/10.1038/s41467-023-36645-3

[31] M. Rahal, B. Denis, T. Mazloum, F. Munoz, R.D. Errico, RIS-aided positioning experiments based on mmWave indoor channel measurements, in: Proc. 2023 13th Int. Conf. Indoor Positioning and Indoor Navigation (IPIN), 2023 13th Int. Conf. Indoor Positioning and Indoor Navigation (IPIN), 2023, pp. 1–6. https://doi.org/10.1109/IPIN57070.2023.10332516

[32] L.P. Joseph, R.C. Deo, D. Casillas-Pérez, R. Prasad, N. Raj, S. Salcedo-Sanz, Short-term wind speed forecasting using an optimized three-phase convolutional neural network fused with bidirectional long short-term memory network model, Appl. Energy 359 (2024) 122624.

[33] Z. Chen, M. Ma, T. Li, H. Wang, C. Li, Long sequence time-series forecasting with deep learning: a survey, Inf. Fusion 97 (2023) 101819.